

Automated Geometric Registration for Multi-Projector Displays on Arbitrary 3D Shapes Using Uncalibrated Devices

Mahdi Abbaspour Tehrani[✉], M. Gopi, and Aditi Majumder

Abstract—In this article we present a completely automated and scalable multi-projector registration system that allows multiple uncalibrated projectors and cameras on arbitrary shape surfaces. Our method estimates the parameters of multiple uncalibrated tiled or superimposed projectors, the extrinsic parameters of the observing cameras (with known intrinsic parameters), the shape of the illuminated 3D geometry and geometrically registers the projectors on it. This is achieved without using any fiducials, even if part of the surface is visible to only one camera. The method uses a completely automatic approach for cross-correlation and cross-validation of the device parameters and the surface geometry resulting in an accurate registration on the arbitrary unknown geometry that does not need an accurate prior calibration of each of the uncalibrated devices using physical patterns or fiducials. Estimating projector parameters allows for quick recalibration of the system in the face of projector movements, by re-estimating only the parameters of the moved projector and not the entire system. Thus, our work can enable easy deployment of spatially augmented reality environments of different sizes (from small table top objects to large immersive environments), different shapes (inside-looking-out or outside-looking in), and different configurations (tiled or superimposed) using the same proposed method.

Index Terms—Automatic projector calibration, visualization systems, multi-projector systems

1 INTRODUCTION

Spatially Augmented Reality (SAR) systems entail lighting using multiple projectors to create high-resolution imagery on physical objects (e.g., a dome, a relief map or a table top object). SAR systems are used in several applications such as gaming, 3D visualization and appearance modification. More often than not, every part of the object cannot be illuminated at the desired resolution using a single projector. Therefore, multiple projectors are usually tiled or superimposed to light all parts of the surface to achieve high pixel density and high brightness. The challenge in such SAR systems lies in creating a seamless imagery on the arbitrarily shaped display surface even though they come from multiple projectors.

In this paper we present a generic, completely automatic geometric registration method that enables illumination of arbitrarily shaped surfaces using m uncalibrated projectors run by p machines and observed by n cameras where the projectors can be either tiled or superimposed. Our method starts with uncalibrated non-linear projectors and unknown surface geometry and recovers intrinsic and extrinsic parameters of projectors, extrinsic parameters of cameras and projector non-linearities and the surface geometry. Note that geometric registration (assuring that the same point on the surface receives identical content from multiple overlapping projectors) does not entail estimating all the device parameters and surface

geometry. Most prior systems achieve geometric registration without estimation of all system parameters. However, estimation of parameters of devices not only enables geometric registration but also can be used to achieve registered imagery during dynamic projector movement or quick recalibration if the surface geometry changes.

1.1 Main Contributions

The main contributions of this work are as follows.

1. Our main contribution lies in a complete consistent recovery of all the parameters of the m projectors and n cameras, the shape of the illuminated 3D surface, and subsequent geometric registration in a multi-projector system using uncalibrated devices without using any fiducials. More importantly, unlike any prior method that need at least two cameras to observe *every* surface point, we can achieve this registration even when parts of the surface are observed by just one camera as long as it is illuminated by a projector. Of course, we do need a minimum of 2 cameras, i.e $n \geq 2$. This significantly simplifies the deployment of the system. Since we recover all the device and surface parameters, we can map any content on the arbitrarily shaped surface in both view-dependent and view-independent (e.g., conformal mapping) manner.
2. Unlike any prior work, we can estimate the parameters for *non-linear* projectors recovering their non-linear distortion parameters, and their intrinsic and extrinsic parameters as well. Recovering intrinsic parameters of a projector are harder than a camera due to the

* The authors are with the University of California Irvine, Irvine, CA 92697 USA. E-mail: mabbasp@uci.edu, {gopi, majumder}@ics.uci.edu.

Manuscript received 6 Apr. 2018; revised 11 June 2019; accepted 16 Aug. 2019. Date of publication 1 Nov. 2019; date of current version 25 Feb. 2021. (Corresponding author: Mahdi Abbaspour Tehrani.)

Recommended for acceptance by D. Schmalstieg.

Digital Object Identifier no. 10.1109/TVCG.2019.2950942

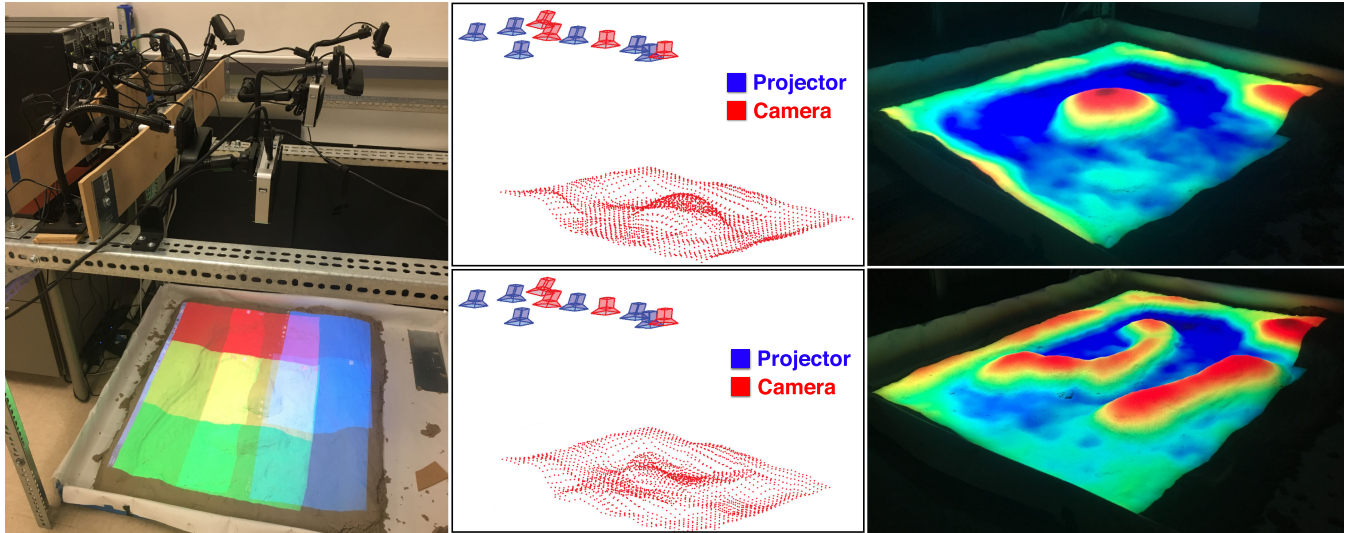


Fig. 1. Left: Our setup made of 6 projectors and 4 cameras illuminating a hand-modelled sand pit, creating a surface of arbitrary shape, each projector shown with a different color. Middle: recovered 3D shape of the sand-pit and parameters of the projectors and cameras for two different shapes. Right: A seamless elevation map projected on the arbitrary shape. Note that the warmer colors light the higher regions and the cooler colors light the lower regions demonstrating the accuracy of our surface geometry reconstruction.

presence of an offset parameter to account for offset projection. This parameter is usually assumed to be zero when recovering camera intrinsic parameters. Further, the difficulty of estimating projector parameters has been well-acknowledged and attributed to the assumption that projectors are linear devices when in reality they, especially commodity ones [1], are usually non-linear. Our method achieves this successfully in a multi-projector system.

3. The novelty of our technique lies in using multiple levels of cross validation across multiple devices and surface geometry to recover the numerous system parameters robustly. Therefore, existence of a large number of devices, which is often viewed as a challenge for any multi-projector system, is exploited effectively to achieve high robustness and accuracy. However, the estimated device parameters may be different than the parameters recovered when calibrating each device separately and independently using physical fiducials. Instead, the estimated parameters provide a consistent model of the entire system that inherently assures scalability. Further, it allows interactive projector movements via tracking of features embedded in the content via the same cameras observing the system. Simultaneously achieving robustness, interactivity accuracy, and scalability when using multiple uncalibrated devices on unknown 3D shapes has been an elusive goal for all existing works on multi-projector displays and we address this effectively in this paper.

2 RELATED WORK

This work focuses on geometric registration and not color registration that deals with spatial variation in chroma and brightness across the display [2], [3]. Also we focus only on white surfaces and not on radiometric compensation for textured surfaces. We compare the proposed method with prior work from three different perspective see Table 1.

2.1 Registration Versus Parameter Estimation

Geometric registration of multi-projector system means, for every pixel of a projector, finding the set of pixels from other projectors overlapping with it on the display surface. This set is non-empty only for pixels in the overlapping region of more than one projector's image on the display surface. Geometric registration can be performed using an observing camera without a full fledged estimation of the intrinsic and extrinsic projector/camera parameters and reconstruction of the 3D surface geometry. Therefore, estimation of all system parameters provides geometric registration as a by-product, but not vice versa.

Only a full estimation of system parameters can allow us to harness the complete potential of two-pass rendering [4] when interfacing with 3D content delivery on multi-projector displays. The estimated projector intrinsic and extrinsic parameters are crucial to compute precisely the images to be projected from each projector.

Closely related to the aforementioned issue of registration is the kind of content mapping that can be provided. View dependent mapping maps the content on the display surface from particular viewpoint. Therefore, view-dependent mapping is only correct for a single static vantage point and may result in visible distortions from other viewpoints. View independent mapping, on the other hand, provides a mapping of the content on the surface that is suitable for multi-user viewing (e.g., wallpapering via conformal mapping).

Geometric registration (instead of a calibration) is sufficient for a view-dependent mapping from a single vantage point. The camera used for registration is placed at the vantage point and the image to be viewed by the viewer is considered to be in the camera's coordinate system. Mapping the image seamlessly from this viewpoint on to the display then entails just picking the content for a pixel of any projector from the registered camera pixel location. But, for view-independent mapping the shape of the surface needs to be recovered or known, which in turn requires recovering or knowing the device parameters of the uncalibrated projectors or cameras seeing

TABLE 1
Comparison of our Work With Previous Works

Method	Projector Calibration	Surface Type	Camera requirement	Scalability	accuracy	Physical Pattern
[5], [6], [7], [8], [9], [10]	✗	planar	1	✓	-	No
Raskar et al. 1999[1]	✓	Arbitrary	2/point	✗	multi-pixel	Yes
Raskar et al. 2003[50]	✗	Quadric	1 camera + 1 tilt sensor / projector	✗	multi-pixel	No
Raskar et al. 2004[19]	✗	Quadric	2	✗	sub-pixel	No
Harville et al. 2006[12]	✗	Developable	1	✓	sub-pixel	No
Brown et al. 2002[11]	✗	arbitrary	1	✗	-	No
Zhou et al. 2008[43]	✓	Arbitrary	1/projector	✗	multi-pixel	Yes
[12], [13]	✗	Cylindrical	1	✓	sub-pixel	Yes
Johnson et al. 2009[48]	✗	Known	2/projector	✓	sub-pixel	No
Sajadi et al. 2009 and 2010[14], [15]	✗	Smooth vertically extruded	1	✓	sub-pixel	No
Sajadi et al. 2010[17]	✗	Swept	1	✓	sub-pixel	No
Sajadi et al. 2011[16]	✗	Domes	1	✓	sub-pixel	No
Sajadi et al. 2010 and 2011[18], [39]	✓	Piecewise smooth vertically extruded	1	✓	sub-pixel	No
Sajadi et al. 2015[21]	✗	Arbitrary	2/point	✓	sub-pixel	No
Our method	✓	Arbitrary	1/point	✓	sub-pixel	No

the surface. The same is required for creating view-dependent images from multiple viewpoints as is necessary in a system where the position of a tracked user changes dynamically. Computing these parameters require estimating all the parameters of the multi projector system.

Comparison with Prior Work. Most prior works propose geometric registration and not full fledged estimation of all the system parameters. Since *planar surfaces* enable relating (linear) projectors via homography, most prior works that use multiple projectors on a flat surface essentially achieve a geometric registration [5], [6], [7], [8], [9] allows projector non-linearities while still achieving only geometric registration. Finally, [10] introduces a distributed radially cascaded method that breaks away from tree-based approach to significantly increase the accuracy, scalability and robustness of registering multiple projectors on a planar display.

When considering *non-planar surfaces*, a large number of methods try to avoid the problem of recovering the surface geometry explicitly thereby achieving only geometric registration [11]. Other works try to use fiducials on cylindrical surface and create a piecewise linear 2D display parametrization in the camera space to achieve the registration [12], [13]. This allows a wall-papering on the 3D surface whose quality is completely dependent on the density of the piecewise linear parametrization dictated by the number of fiducials used. Though these systems are motivated by the objective of generating a simple system with minimal use of cameras, they introduce perceivable distortions when viewed from a different vantage point than the camera, the distortions being more perceivable as the distance between the camera position and the view position increases. Further, only view dependent mapping from a single vantage point can be achieved.

A body of work [14], [15], [16], [17], [18] shows that for a class of non-planar shapes whose category and approximate measurements are known apriori (e.g., vertically extruded surfaces whose height and aspect ratio can be measured, domes whose radius can be measured), the simplicity of a single uncalibrated camera can be retained (without using stereo cameras) and the geometry of the display surface can be recovered at the same time. This 3D geometry recovery enables both view-independent content mapping and view-

dependent content mapping from any view point. Later works break free from single camera and use stereo cameras for reconstructing the geometry of special kind of surfaces called quadric surfaces (e.g., spheres, cylinders, ellipsoids and paraboloids) [19], or a corner of a room [20]. However, since projection parameters are not estimated in any of the aforementioned works, two-pass rendering and easy reconfiguration is still not possible.

Our work is closest to multi-projector systems on arbitrary non-planar shapes that are observed by multiple cameras. One of the earliest works in this direction [1] uses tightly coupled centralized method to achieve geometric registration using custom-built 3D fiducials (e.g., checkered cubes) and has the following steps. (a) It is assumed that every point on the surface is seen by at least two cameras. These cameras are calibrated using the 3D fiducial. (b) Structure light patterns from the projectors are then used by each calibrated camera to reconstruct a part of the display surface. (c) These partial reconstructions are then stitched together with respect of one camera's coordinate system to create the entire 3D geometry. (d) The known 3D geometry and the correspondences recovered via structured light are then used to achieve the multiple projector registration. Since no cross-validation is applied, the model created by the independently estimated device parameters is not consistent with each other or the recovered 3D surface resulting in severe accumulation of error across different devices and poor accuracy of registration. Most recently, [21] uses a technique similar to [1] while surface reconstruction is improved via a centralized technique using cross-validation across multiple cameras yielding a more accurate reconstruction. More recently, [22], [23], [24], [25] have developed similar centralized 3D reconstruction method to achieve registration on complex 3D shapes, but without using any fiducials. To constrain the system sufficiently, these methods use *completely superimposed projectors* and validate the results from photometric and geometric stereo, resulting in self-calibrating systems. However, note that all these aforementioned works merely address geometric registration and does not strive to estimate the projector intrinsic and extrinsic properties, the camera parameters and the surface geometry in a consistent manner.

It has been identified that commodity projectors cannot be modeled as a dual of a linear camera [26]. Some prior works achieve projector calibration in small single projector-camera systems [27], [28] and most of these works use physical planar or 3D calibration patterns (e.g., a checkerboard) and therefore can not be automated [29], [30], [31], [32], [33], [34], [35], [36], [37], [38], [39] is the only work in the multi-projector display domain that addresses the issue of automated projector calibration, but only when projecting on a cylindrical geometry while assuming a linear projector model. Therefore, [39] cannot be used for varied surface geometries. [40] estimates the parameters of multiple projectors using a planar sheet used as calibration target and this calibration target has to be placed at different positions and orientations during the calibration process. [41] estimates the extrinsic parameters of multiple projectors by having the intrinsic parameters of all projectors and cameras. [42] addressed the automatic calibration of multi-projector-camera systems and shows scalable result which is comparable with standard checker-board calibration method. The goal of this work is accurate intrinsic and extrinsic calibration of devices without considering the problem of geometric registration in multi-projector displays unlike our work whose focus is the accurate registration across multiple projectors.

Most prior work focus on specific configurations or setups [1], [19], [39], [43] and fail to provide a method that can scale to a general system of m projectors, n cameras where pre-calibrating each of the $m + n$ devices is cumbersome and difficult. Unlike any earlier systems, we demonstrate the scalability of our system to a large number of devices and very general display shapes. Since we recover the unknown display shape and all the parameters of the uncalibrated devices (including non-linear distortion parameter for projectors) together, we can create very large multi-projector systems easily.

2.2 One-Time Versus Continuous Registration

Both geometric registration and calibration require pixel correspondences between projectors and cameras that are obtained by projecting a sequence of structured light patterns from the projectors while capturing them with the cameras. Therefore, any change in the system such as a projector movement or a change in the shape of the 3D surface requires computing new correspondences by either (a) disrupting content projection by reprojection and recapture of the structured light patterns; or (b) using the features embedded in the content thereby causing no disruption.

Comparison with Prior Work. All the aforementioned works so far have focused on one-time calibration which is usually repeated every time anything changes in the system. Continuous calibration has been addressed so far only on smaller *single projector* systems. Yang and Welch [44] assumes a single calibrated projector-camera pair and monitor the projected content (as opposed to special structured light patterns) continuously to estimate the change of the shape of the surface (e.g., a moving cloth) and compensate the projected image to account for it. Using a projector augmented by two stereo cameras, Cotting et al. [45], [46], [47] embeds imperceptible structured light patterns in the projected imagery to estimate the shape of the display surface and the pose of a single projector continuously. Zhou et al. [43] achieves the same by tracking displayed image features. Johnson et al. [48] shows that

multiple such single-projector-two-camera units can be used in a distributed framework to achieve continuous calibration in a multi-projector setup if the geometry is known. Zollman et al. [49] uses optical flow techniques to present a hybrid technique that can compensate for small changes in display configuration for small changes in optical flow and resort to active structured light projection only when optical flow results are unreliable due to large changes in the display configuration. Their system is designed for correcting the image from a view of a moving observer, but the single projector is static. In our system we show the result of moving the projector itself in a multi-projector system.

2.3 Scalability, Accuracy and Robustness

When considering multi-projector systems, effectiveness and ease in deployment of a method is crucially dependent on the accuracy, scalability and robustness of the method. This is where we make the most significant contribution.

Accuracy. Unlike other computer vision systems that reconstruct 3D geometries for visualization purposes, the accuracy requirement of 3D reconstruction for the purpose of projecting on top of it from multiple projectors is much more challenging. This is because even a single pixel error in the reconstructed surface or the intrinsic and extrinsic device parameters manifests themselves as highly visible mis-registrations in the displayed imagery.

Scalability. Scalability of a method is the ability to produce accurate results on a large number of devices, large size of display and large variability of display shapes.

Robustness. Robustness refers to the ability of a system to deliver accurate results *consistently* over time in face of changes in number of devices and shape of the display.

Comparison with Prior Work. Several complex procedures, most often involving multiple fiducials on the display surface, are used to achieve camera calibration and 3D display reconstruction [1], [12], [13], [43], [45], [46], [47], [48]. However, these methods usually demonstrate their registration result for relatively simpler system configurations avoiding intersection of more than two projectors in the overlap area or a cycle formed via a relationship of overlap between the projectors that can cause inconsistencies (e.g., the concatenated transformations across a loop is not identity) and therefore large accumulated errors. Some prior work [21] cross validate the 3D reconstruction across multiple cameras thereby increasing the robustness of the surface reconstruction process without addressing projector parameter estimation at all. In contrast, our method leverages multiple rounds of cross-validation in a distributed fashion to achieve a hitherto unseen robustness. All prior systems operate under the constraint that every point on the arbitrary 3D shape is observed by at least two cameras to allow the global centralized multi-view reconstruction of 3D shape [21]. Further, these methods only recover the mapping between the projector space and the 3D surface instead of recovering the intrinsic and extrinsic parameters of the projector. Therefore, recalibration, if the projector is moved, requires running the whole process of 3D reconstruction and projector registration again even if the projection surface is unchanged and only projectors are moved. Unlike [1], [19], [20], [22], [23], [45], our method works as long as a display surface point is observed by at least one camera, making our system unconstrained, scalable, easy to deploy, and robust.

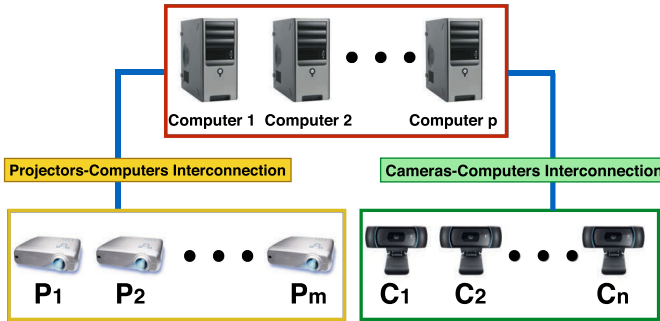


Fig. 2. The system with n cameras and m projectors connected to p computers via two independent interconnection networks.

3 SYSTEM OVERVIEW

Our system consists of m projectors tiled or superimposed to illuminate an unknown 3D surface S observed by n cameras connected in a distributed network (Fig. 2). P_i denotes projector i , $1 \leq i \leq m$ and C_j denotes camera j , $2 \leq j \leq n$. The m projectors and n cameras are connected to the computers via interconnection network I_p and I_c respectively. They illuminate an arbitrary shaped surface S whose 3D coordinates are denoted by (X, Y, Z) . We assume that every point on S is illuminated by at least one projector and observed by *at least one* camera and only a small portion of the projection area of each projector (at least %20 of projection area) has to be seen by at least two cameras. One common configuration that easily enforces this constraint is pairing every projector with a camera (i.e., $m = n$) assuring a baseline between them. Since the camera field of view (FOV) is usually wider than a projector, this assures that every point on S is seen by at least one camera as long as every point on S is illuminated by at least one projector. However, since today's camera FOV are usually much larger than that of projectors', it is fairly easy to set up a system where $n < m$. Also, note that we do not impose any constraint against completely superimposing projectors. Fig. 3 shows a system with $m = 6$, $n = 4$, that satisfies these assumptions.

We assume that we know the focal length f_j of camera C_j . In practice, this is achieved by procuring f_j from the image meta-data. This is a standard practice today with almost any computer vision technique [39], [51], [52]. Further, as in [39], [53], we assume the principal center of the camera to be coincident with the center of the image plane, no skew between the image axes, and square pixels. Such assumptions are practical in almost all commodity cameras. Therefore, the intrinsic matrix K_j^c for camera j is given by

$$K_j^c = \begin{pmatrix} f_j & 0 & 0 \\ 0 & f_j & 0 \\ 0 & 0 & 1 \end{pmatrix}, \quad (1)$$

where f_j is the focal length of the camera C_j in pixels.

Since most practical projectors come with small non-linearities [54], [55] we use a non-linear model for the projector to account for the radial and tangential distortions that is given by combining a non-linear model with a linear model. Let us assume E_i is the extrinsic matrix for projector P_i . Then the normalized pinhole projection of 3D point (X, Y, Z) , using a linear camera model, is given by $(x_i, y_i) = (\frac{X'}{Z'}, \frac{Y'}{Z'})$ where

$$\begin{pmatrix} X' \\ Y' \\ Z' \\ 1 \end{pmatrix} = E_i \begin{pmatrix} X \\ Y \\ Z \\ 1 \end{pmatrix}, \quad (2)$$

Augmenting the non-linear model to the above equation to account for the non-linearities, we get

$$\begin{pmatrix} x'_i \\ y'_i \end{pmatrix} = (1 + \alpha_i^1 r_i^2 + \alpha_i^2 r_i^4 + \alpha_i^3 r_i^6) \begin{pmatrix} x_i \\ y_i \end{pmatrix} + \begin{pmatrix} 2\alpha_i^4 x_i y_i + \alpha_i^5 (r_i^2 + 2x_i^2) \\ \alpha_i^4 (r_i^2 + 2y_i^2) + 2\alpha_i^5 x_i y_i \end{pmatrix}, \quad (3)$$

where α_i^1, α_i^2 and α_i^3 are radial distortion coefficients and α_i^4 and α_i^5 are tangential distortion coefficients for projector P_i and $r_i = \sqrt{x_i^2 + y_i^2}$. Therefore, the final coordinate of the 3D point in projector's image plane is given by $(p_i, q_i) = (\frac{x''_i}{z''_i}, \frac{y''_i}{z''_i})$ where

$$\begin{pmatrix} x''_i \\ y''_i \\ z''_i \end{pmatrix} = K_i^p \begin{pmatrix} x'_i \\ y'_i \\ 1 \end{pmatrix}, \quad (4)$$

where K_i^p is the intrinsic parameter matrix of the projector P_i given by

$$K_i^p = \begin{pmatrix} f_i^p & 0 & u_i \\ 0 & f_i^p & v_i \\ 0 & 0 & 1 \end{pmatrix}, \quad (5)$$

where f_i^p, v_i and u_i are the focal length, vertical and horizontal offset in pixels respectively. These parameters are required to model the offset projection feature available in most commodity projectors.

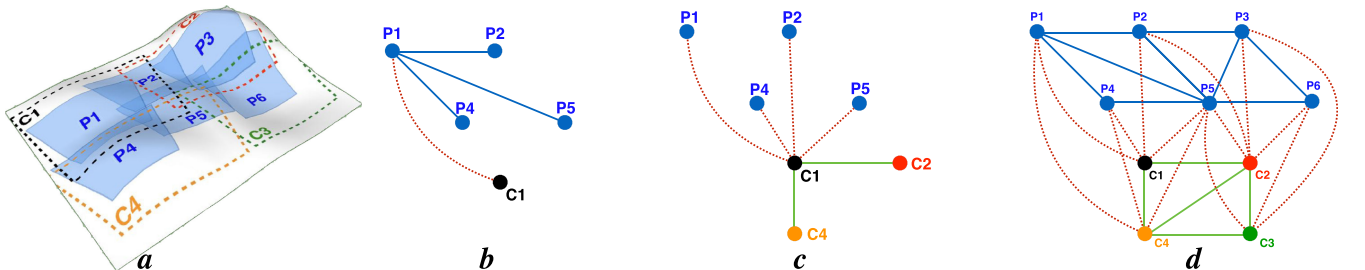


Fig. 3. (a): The configuration of a system with 6 projectors 4 cameras. Each blue region shows the projection area of a projector and dashed colored lines show the FOV of the cameras. (b and c): local adjacency graph for P_1 and C_1 constructed by C_1 . The edges of partial A_p and A_c are shown in blue and green respectively. The cross edges are shown with red dashed lines. The nodes of the A_c are color coded to be consistent with the camera field of views shown in (a). (d): The connectivity graph between projectors and cameras. Note that many regions of the surface is seen by only one camera. For example, most of P_3 is seen only by C_2 . Similarly, most of P_1 is seen only by C_1 .

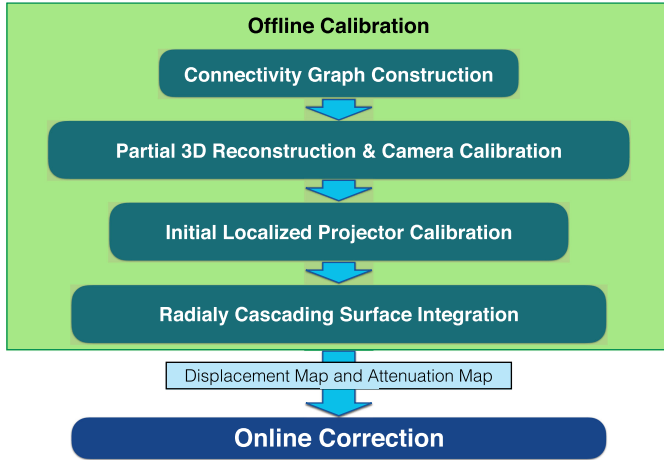


Fig. 4. This figure shows the pipeline of our method. Our method has two components. First an offline calibration algorithm provides the displacement and attenuation map, then our online correction algorithm uses these maps to create a seamless imagery on the arbitrary shape.

Our method comprises of an *offline calibration* followed by an *online image correction* (Fig. 4). The offline calibration recovers display surface and geometric parameters of each device (projector and camera) which are used to create a displacement map for each projector. These displacement maps are then used in the online image correction phase (Section 5) to warp the geometry of the images projected by each projector in real-time. For color calibration, the parameters recovered in the offline calibration are used to create per projector attenuation maps that are applied after the displacement map in the online image correction phase to achieve simple edge blending [1] in the overlap regions to smooth color transition between the projectors. The result is seamlessly registered imagery on an arbitrarily shaped surface S .

4 OFFLINE CALIBRATION METHOD

Our auto-calibration offers a distributed method that comprises of the following four steps:

- 1) *Connectivity graph construction* finds the connectivity between devices in the context of their overlapping field-of-view,
- 2) *Partial 3D reconstruction and camera calibration* step recovers the camera parameters and the shape S of the surface partially in regions that are seen by more than one camera,
- 3) *Initial localized projector calibration* achieves initial estimation of the linear and non-linear projector parameters using the partially-reconstructed display surface S and the camera parameters,
- 4) *Radially cascading surface integration* step refines the recovered projector parameters and integrate the 3D reconstruction of parts of S .

The above four steps yield complete reconstruction of S and an accurate calibration of all the devices.

4.1 Connectivity Graph Construction

Connectivity graph provides information about the overlap between the camera and projector field of views and we recover this graph automatically. Many prior work [8], [56]

that achieve projector calibration in multi-projector displays assume that the projectors and cameras form a regular grid. We avoid any such assumptions that are difficult to ensure in practice. However, we do assume that the connectivity graph is static and does not change during the calibration process.

The connectivity graph, A , is an undirected graph consisting of two sub-graphs: a *camera adjacency graph*, A_c , and a *projector adjacency graph*, A_p , with cross-edges between these two sub-graphs. Each node in A_c indicates a camera and an edge between u and v , $u, v \in j$, denotes that the FOV of C_u covers more than a fraction α , $0 < \alpha < 1$, of the FOV of C_v and vice versa. Typically, we set $\alpha = 0.2$ (a 20 percent overlap between cameras) to assure robust use of structure from motion (SfM) techniques, well known computer vision technique used for this purpose [57], [58]. Similarly, each projector is represented by a node in A_p and an edge between e and f , $e, f \in i$, denotes an overlap between P_e and P_f . Finally, we define *cross edges* between A_p and A_c . A node u in A_c is connected to a node e in A_p , $u \in j$ and $e \in i$, if C_u sees whole or part of P_e . Fig. 3 shows an example of the connectivity graph of a system with six projectors and four cameras.

To construct A , each projector in the sorted order of their IP address projects white and the scene captured by all cameras after each projection.

Each camera C_j constructs the local adjacency around itself and the adjacency around each projector it observes using all the captured images (Fig. 3b and 3c shows the local adjacency graph for P_1 and C_1 constructed by images captured by C_1). Next, the camera broadcasts the part of A it has constructed to all the projectors. Each projector consolidates the different parts of A it receives from all cameras to construct the complete adjacency information. Fig. 3d shows an example of the final connectivity graph between projectors and cameras.

4.2 Partial 3D Reconstruction and Camera Calibration

The goal of this step is to reconstruct the geometry of the part of S that is seen by two or more cameras and also recover the camera extrinsic properties. This is therefore a SPMD (single program multiple data) process conducted on each projector P_i in parallel in a distributed manner.

The process proceeds in K iterations ($K \leq m$). In the k th iteration, $k < K$, a set of *non-overlapping* projectors, W_k , that forms a subgraph of A_p , project a set of binary blob patterns and all the cameras adjacent to W_k in A , capture the images. The exact value of K depends on the connectivity of sub-graph A_p . Densely connected graphs, indicating larger connectivity in A_p , results in higher values of K . In the worst case, $K = m$, where each projector projects the patterns sequentially.

The set of sets of non-overlapping projectors is computed using a greedy algorithm. All the projectors are tagged UNMARKED in the beginning of the algorithm. To choose the set of projectors W_k in iteration k , W_k is initialized to null set and the UNMARKED projector with the lowest ID that has no connectivity with W_k grabs the token, includes itself in W_k , changes its status to MARKED and then releases the token. This continues till all the UNMARKED projectors have a adjacent projector in W_k . In iteration k , all the projectors in the set W_k project binary blob patterns to use for 3D reconstruction. The above process continues

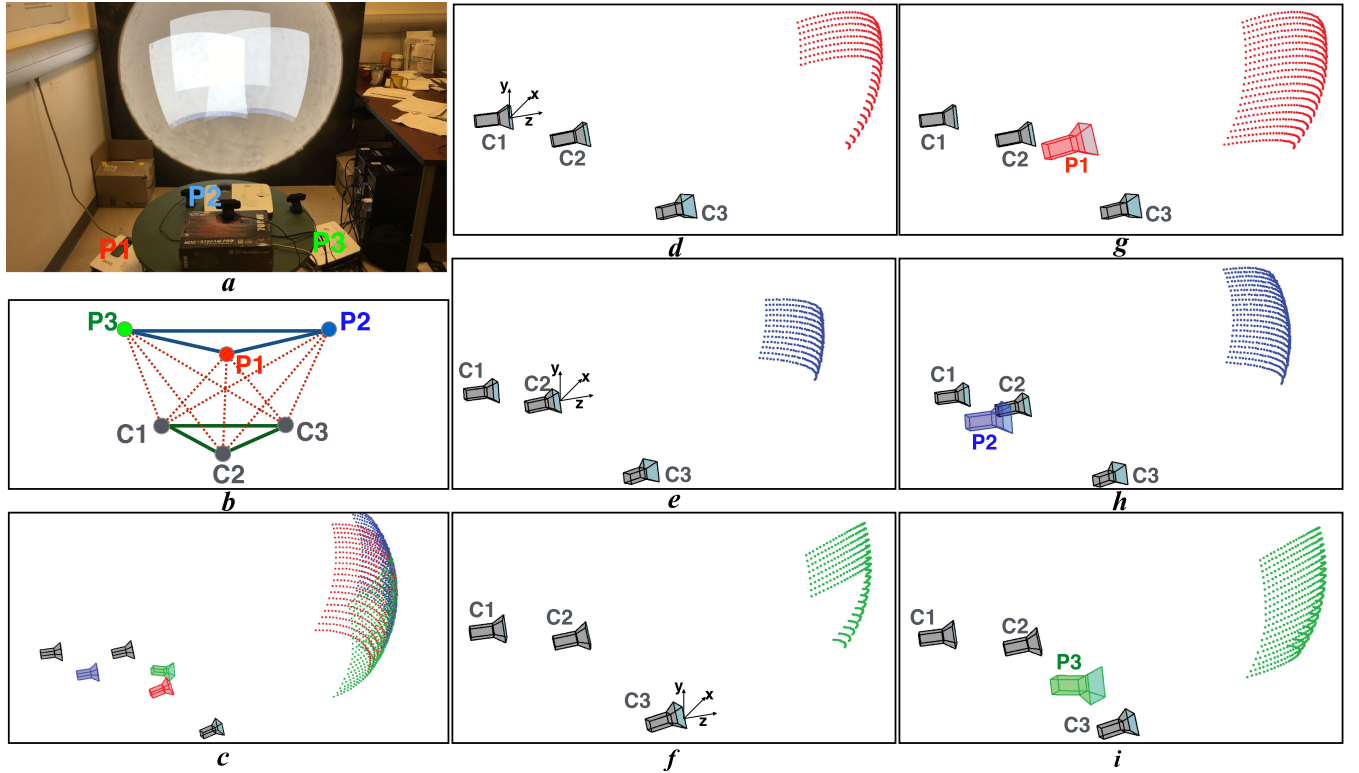


Fig. 5. This figure shows steps of our algorithm. (a): Our setup with 3 projectors and 3 cameras on a dome. (b): Adjacency graph for projectors and cameras. (d, e, and f): Camera calibration and partial 3D reconstruction for 3 projectors after Step 2. (g, h, and i) Complete 3D reconstruction of the display surface of P_1 , P_2 , and P_3 in red, blue, and green respectively after step 3. Each of these 3D reconstructions are in different coordinate systems with different rotation, translation and scale factors. (c): The 3D reconstruction of the display surface, and the calibrated projectors after Step 4 of radially cascading refinement.

through next iteration until all projectors are MARKED. These blobs are used to find correspondences across multiple devices. The density of blobs to be used depends on the smoothness of the display surface—smoother surface requiring sparser blob density. The basic assumption is that the surface changes smoothly between two projected blobs.

Algorithm 1.

- 1: **procedure** PARTIAL 3D RECONSTRUCTION
- 2: $G \leftarrow$ Set of cameras in A_c adjacent to P_i in A_p connected via the cross edges.
- 3: Designate $C^R \in G$ with the maximum connection with other cameras in G as reference camera for P_i .
- 4: $D \leftarrow \{C^R\}$
- 5: $G \leftarrow G - \{C^R\}$
- 6: **while** G is not empty **do**
- 7: Select $C_i \in G$ with the maximum connectivity with D .
- 8: $D \leftarrow D \cup \{C_i\}$
- 9: $G \leftarrow G - \{C_i\}$
- 10: Find $C_u \in D, u \neq i$, that has overlap with C_i .
- 11: Use correspondences between C_i and C_u in a structure from motion (SfM) method to (1) reconstruct the extrinsic parameters of C_i and C_u ; and (2) the 3D geometry of the surface seen by both C_i and C_u .
- 12: $C_i^a \leftarrow$ set of all cameras in D that are adjacent to C_i in A_c .
- 13: Perform a bundle adjustment optimization using all cameras in C_i^a refining their extrinsic parameters.
- 14: Refine the 3D reconstruction of part of S seen in overlapping FOVs of cameras in C_i^a using all the correspondences from all pairs of cameras.

The captured images of the patterns projected by each projector P_i give us a set of correspondences between P_i and its adjacent cameras which are then processed as described in Algorithm 1 to reconstruct the camera extrinsic parameters and regions of S seen by at least two cameras. The parts of S seen by only one camera will not be reconstructed in this step.

Using the mentioned steps in Algorithm 1, we have now reconstructed the part of S illuminated by P_i that is seen by two or more cameras which are also calibrated during the process. We denote this part of the surface as S_{P_i} . However, this reconstructed region is in the local coordinate system defined by C^R . Fig. 5d, 5e, and 5f show partial 3D reconstruction of surface for three projectors. Notice that each of these figures is in local coordinate system based on the reference camera. For example, in Fig. 5d, 5e and 5f, C_1 , C_2 and C_3 are the reference cameras respectively.

4.3 Initial Localized Projector Calibration

The result of the previous step leads to a set of correspondences between 2D projector coordinates of P_i , (x_i, y_i) , and the 3D coordinates of S_{P_i} , denoted by (X_i, Y_i, Z_i) . From these correspondences we solve a non-linear optimization for each P_i using maximum likelihood estimation via Levenberg Marquardt algorithm [59] to estimate K_i^p , E_i and α_i^k for $k = 1, 2 \dots 5$ and thus calibrate each projector P_i . When achieving projector calibration, if all the points lie on a single plane, it will be a degenerate case for our method. Therefore, though we can handle partial planar region (as long as it does not cover the entire field of view of a projector), for a

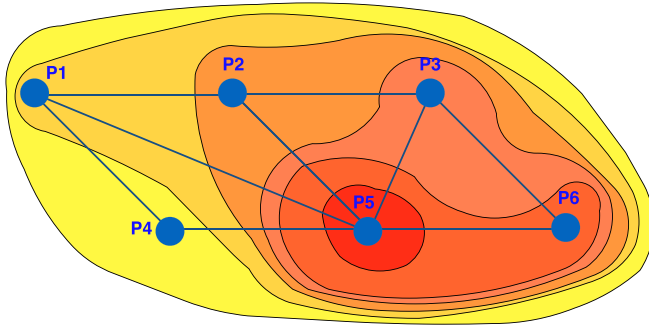


Fig. 6. This figure shows the order that projectors added to set V from our previous example in Fig. 3. The gradient of the color from red to yellow shows the order of the projectors - $P_5, P_6, P_3, P_2, P_1, P_4$.

completely planar displays a large number of prior homography based methods can be used [56], [60], [61], [62], [63].

Following the projector calibration, for every surface point of S illuminated by P_i , we can find the correspondences in one or more calibrated cameras. Therefore, we can perform a multi-view 3D triangulation to find the 3D position of the center of each blob projected by P_i . To undo the non-linear distortion due to the projector, we use the recovered α_i^k , $k = 1, 2 \dots 5$, to remove the projector non-linearities before applying the multi-view 3D triangulation. Since this step is also performed locally by each P_i , we recover the surface geometry illuminated by each P_i in its own local coordinate system as shown in Fig. 5g, 5h and 5i. The 3D reconstruction of the surface illuminated by each projector is shown with different colors. However, these reconstructed regions are not connected to each other since each of them are still based on the local coordinate system of each projector.

4.4 Radially Cascading Surface Integration

Finally, we integrate the reconstructed parts of S from all the different projectors with respect to one reference projector using a *radially cascading* mechanism inspired by [56] as described in Algorithm 2. We set the projector with maximum number of overlaps with other projectors as the reference projector and denote it as P_r . We denote the set of devices that are integrated with each other as V . Therefore, at this point $V = \{P_r\}$. Then at each step we choose a device (projector or camera) D_s as described in Algorithm 2 and merge the display formed by the device (part of display seen by the device) in V and D_s . Fig. 6 illustrates the order of the projectors added to the set V for an example graph A_p . In every step, the display formed by the devices in V is registered.

For integrating D_s with V we consider all the overlaps of D_s with other devices in V . Then we solve a non-linear optimization problem to find the scale factor γ and refine the extrinsic parameters of D_s to align reconstructed 3D points in the overlap areas of D_s and V . The objective function Err_s minimizes the sum of the distances of the all corresponding 3D points M_i and M'_i in the overlap of D_s and V (M_i and M'_i are 3D coordinates of point i in coordinate system P_s and V) is given by

$$Err_s = \min \sum_{i=1}^N |M_i - (\gamma R_s M'_i + T_s)|^2, \quad (6)$$

where R_s and T_s are the rotation and translation matrices of D_s , respectively, and N is the number of corresponding points in overlap of D_s and V . We use Procrustes analysis described in [64], [65] to solve this problem.

The above step assures that D_s is connected to the display formed by all the devices in V . However, there is no guarantee that the overlap regions between D_s and all the other devices are represented consistently and similarly across all these devices. Therefore, we consider all the projectors and cameras that overlap with D_s and reconstruct the display surface across these devices to form a consistent display surface geometry. This assures that the overlap regions of multiple projectors in V are represented consistently. Fig. 5c shows the integration of the display geometry reconstructed by all the projectors.

Algorithm 2.

```

1: procedure RADIALY CASCADING SURFACE INTEGRATION
2:  $P_r \leftarrow$  The projector with the maximum degree in  $A_p$  (i.e., the projector with most overlaps with other projectors)
3: The coordinate system of  $P_r$  is set as the global reference coordinate system.
4:  $V \leftarrow \{P_r\}$ 
5:  $H \leftarrow \{\text{All Devices}\} - V$ 
6: while  $H$  is not empty. do
7:    $D_s \leftarrow$  The device in  $H$  with maximum number of edges to devices in  $V$ .
8:   Integrate 3D reconstructed points of  $D_s$  with  $V$ .
9:   Refine reconstructed geometry
10:   $V \leftarrow V \cup \{D_s\}$ 
11:   $H \leftarrow H - \{D_s\}$ 

```

At the end of the Algorithm 2, V is the set of all projectors and we have identical 3D representation of display surface along with the estimation of parameters for all the cameras and projectors assuring perfect and consistent registration. Note that since there is no metric scale during the calibration process, the final estimation of device parameters and 3D point coordinates are up to scale. However, much more importantly, the scale factor is consistent across all the m projectors and n cameras. For color correction, we apply simple edge blending described in [1]. The blending is encoded as a per pixel per channel attenuation map for each projector.

5 ONLINE IMAGE CORRECTION

The one-time calibration step generates a per-pixel displacement map and a per-pixel attenuation map for each projector. It also defines the specific part I_i of the global image that should be cut out for each projector P_i . The displacement map defines how every pixel needs to be displaced to achieve geometric registration while the attenuation map defines how each pixel should be attenuated to achieve edge blending.

In the online image correction step, we cut out the appropriate image I_i for each projector P_i , warp I_i using the displacement map and blend them using the attenuation map. These cut, warped and blended images when projected together from multiple projectors create a seamless image on the display surface. This correction is achieved in real-time using the GPU fragment shaders as in [3], [9], [14].

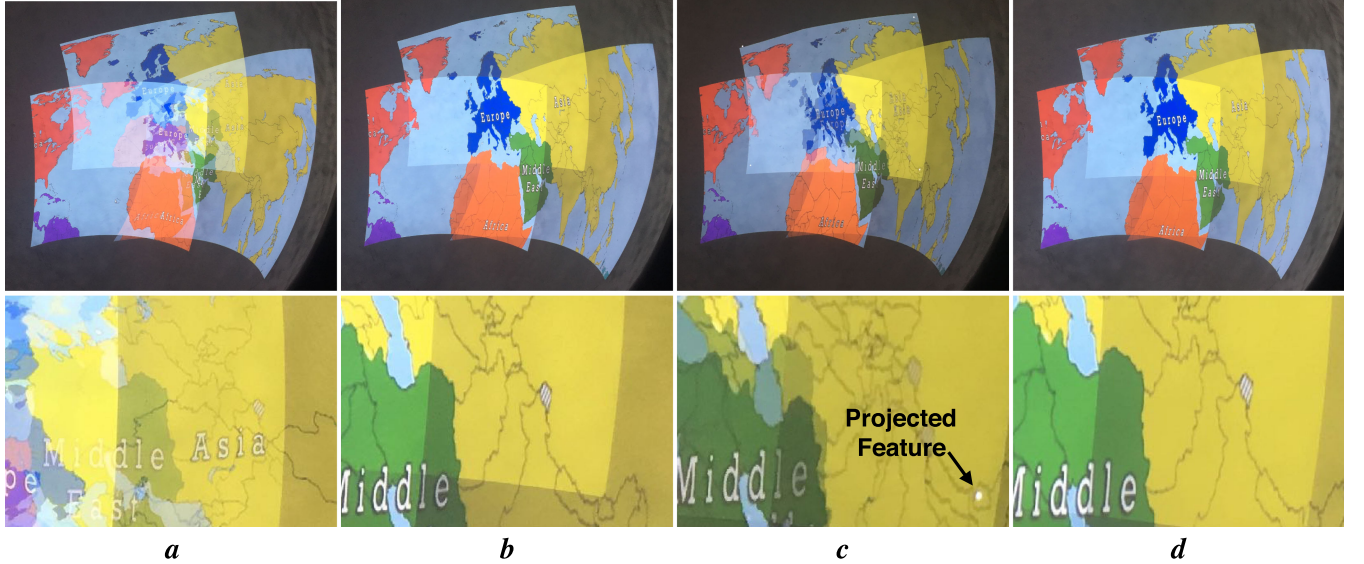


Fig. 7. (a): Projected image with 3 projectors before correction. (b): Geometrically registered image with these 3 projectors. (c): Distorted image after moving a projector. (d): Corrected image after projector recalibration.

As we discussed before, we can achieve *view-independent* or *view-dependent* geometric registration of projected content. Since we reconstruct the shape of S , the image can be wallpapered on S resulting in a *view-independent* correction for multi-user applications. A simple example is indicating the height of the points in a relief map using different colors. Another example is pasting different map layers over the surface, e.g., satellite imagery, road map, or traffic map. These examples are demonstrated in Figs. 1 and 8. In *view-dependent* applications the image can be registered from any arbitrary viewpoint of a moving user. To achieve a *view-dependent* registration for single user applications, we first define the virtual camera (or viewpoint) with projection matrix M . Note that this can be different from the viewpoint of any of the calibrating cameras. Next we use the standard two-pass rendering approach in [4]. First, we render the 3D scene from this virtual camera using M . To generate the image I_i for each projector, at any pixel (x_i, y_i) we find the corresponding 3D coordinates of the surface geometry at (x_i, y_i) . Then we project this 3D point using M to find the corresponding pixel from the image rendered in the first pass. We use the color at this pixel to generate the image I_i .

6 CONTINUOUS REGISTRATION

Our system is capable of adapting to any change in the set up such as projector movement or change in the shape of the display surface. It is practical to assume that such changes occur one at a time instead of concurrently. In this section we explain our method for recalibrating the system for the aforementioned changes in the set up.

6.1 Projector Movement

Unlike any prior work on multi-projector systems, since we calibrate the projector, we do not need to recalibrate the entire system when a projector moves. It is sufficient to just recalibrate the projector P_i that moved. When the projector movement happens, only its extrinsic parameter matrix E_i changes. Therefore, during the projector movement, we embed a few

distinct features in the projected image (During this process the projectors can project a static image or a video). These features are seen by one or more cameras from which the corresponding 3D coordinates in S are deciphered. Using this data, we run the third step of our method (Section 4.3) to find the new extrinsic parameters and recalibrate the projector.

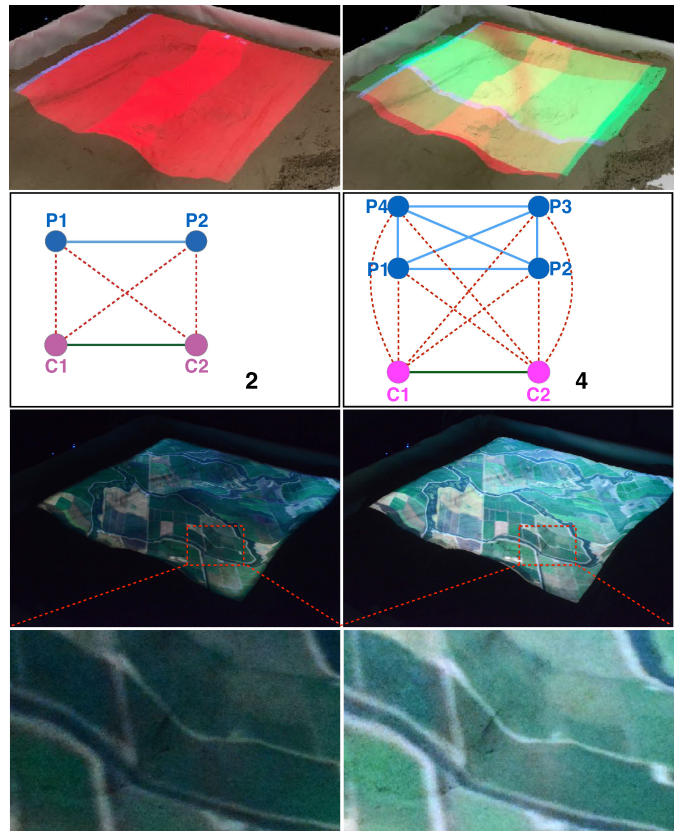


Fig. 8. Top: Our setup with 2 projector (left) and 4 projector for superimposed projection (right). Middle: Connectivity graph of the setups. Bottom: Result with two projectors (1×2 array) (left) and super imposed projection with 4 projectors (2×1 array on a 1×2 array) (right).

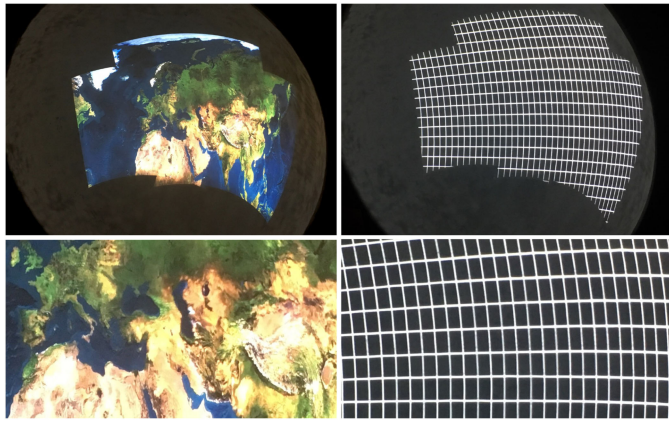


Fig. 9. Final result of projecting on a dome with 3 projector and 3 cameras (top) and zoomed in image (bottom).

Assuming there is no zoom change during the projector movement, projecting only four features at the four corners of the moved projector results in an accurate and fast recalibration. Larger number of features will be required to achieve similar accuracy in the face of zoom changes which can compromise the speed of recalibration slightly. However, these can all be implemented in GPU to run in interactive rates. Further, features embedded in the content itself can be tracked using SIFT feature extraction to achieve the same recalibration without the projection of additional features.

6.2 Changing Display Surface Geometry

If the shape of parts of the surface changes, our system can trigger reconstruction of only the modified part of the surface. This process has two steps: (1) detection of the changes in shape and (2) 3D reconstruction of the affected regions of the surface.

Detection. We assume that the cameras are monitoring the surface via continuous capture. Since all the device parameters, the surface geometry and the content to be projected are known, the image captured by each camera can be predicted. If the captured image differs beyond a noise dependent threshold from the expected captured image, a surface modification is detected. In other words, camera C_i detects a set of pixels U_i that do not have the expected values and thus reflect a change in the shape of the surface.

Reconstruction. Let $F_{j,i}(x_j, y_j) = (u_i, v_i)$ denote that pixel (x_j, y_j) of P_j corresponds to pixel (u_i, v_i) of camera C_i . From this correspondences, we compute the set of pixels U'_j from P_j that corresponds to the set of pixels U_i from C_i as

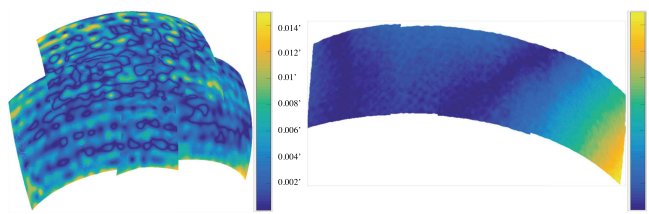


Fig. 10. This figure shows the comparison of the result of 3D reconstruction with ground truth data. The color of each point shows the error of the 3D reconstruction. Left: reconstruction of dome with 5' diameter and the average error of reconstruction is 0.0091' which is %0.0018 of the dome's diameter. Right: reconstruction of a partial cylinder of 14' radius and the average error is 0.021' which is %0.0015 of the cylinder's radius.

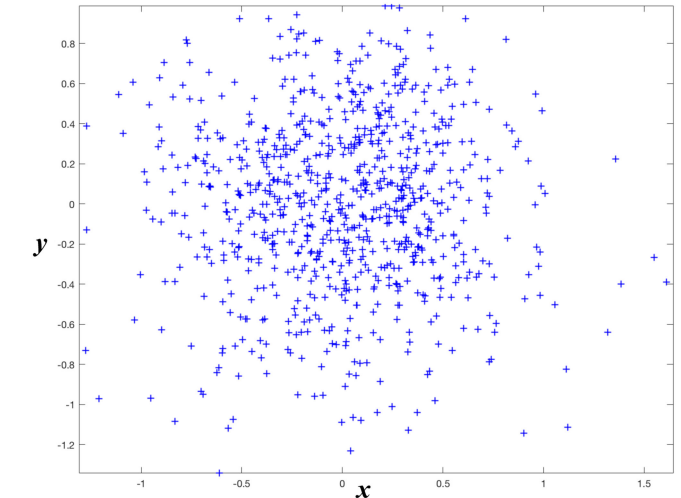


Fig. 11. This figure shows the reprojection error (in pixel) of the 3D points on the projectors image plane in x and y direction in our simulator.

$$U'_j = \{(x_j, y_j) | \exists i, F_{i,j}(x_j, y_j) \in U_i\}, \quad (7)$$

P_j then projects a sequence of structured light patterns in the area covered by U'_j to find a new set of correspondences between P_j and all the cameras. Having these new set of correspondences we can run the last step of our method (section 4.4) to compute the new 3D geometry of the surface.

7 IMPLEMENTATION AND RESULTS

We have implemented our method in four real systems. They come in different sizes (from large area immersive displays to table top objects), different shapes (from cylinders to domes to completely arbitrary surfaces made of sand), for different number of devices, and for both superimposed and tiled projector configurations. This demonstrates the generality and scalability of our method.

The first system is a hemisphere of diameter 5' lit by three projectors (BenQ W1070) in a tiled configuration, seen by three cameras (Logitech c920) and run by three machines ($m = 3, n = 3$ and $p = 3$). Fig. 9 shows our result for this system. The projected grid shows the accuracy of our geometric registration in overlap of all projectors. Fig. 10 shows the accuracy of the 3D reconstruction of the display surface. For obtaining the ground truth data we used a half dome with known 3D shape. The average reconstruction error is 0.0091' which is %0.0018 of the dome's diameter.

The second system is a sand-pit of size 4' \times 3' lit by an array of two, four and six projectors (Qumi Q2-B) in three different set-ups in both tiled and superimposed configuration seen by four cameras (Logitech c920) and driven by three machines i.e., $p = 3, n = 4$ and $m = 2, 4$ and 6. Fig. 1 shows our result with six projectors and 3D reconstruction of the display surface. We show two different arbitrary geometries on the sandpit to emphasize the generality of our method. Fig. 1 shows view-independent geometric registration and Fig. 12 shows the view-dependent geometric registration using four projectors. Fig. 13 shows our system with six projectors. The first column of Fig. 13 shows the view-dependent geometric registration from two different view points and the grid shows the accuracy of our geometric registration. The Third column of Fig. 13

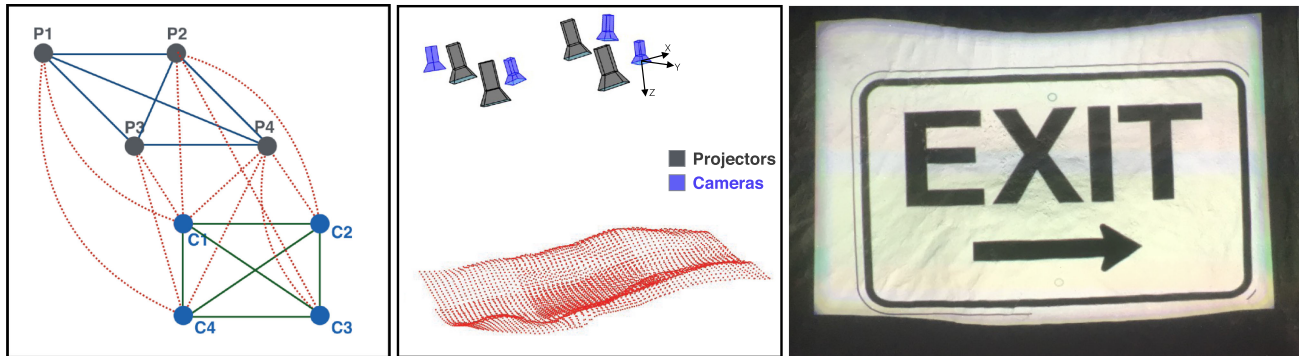


Fig. 12. This figure shows our result projecting on a sand pit with 4 projectors and 4 cameras. Left: Connectivity graph for projectors and cameras. Middle: Recovered 3D geometry of the display surface and parameters of the projectors and cameras. Right: Final result.

shows how we can change the appearance of display surface as we know the 3D geometry of the surface. Fig. 8 shows our result of superimposed projection to increase the brightness of the image. The sandpit is first lit by a 1×2 array of two projectors which are then superimposed by a 2×1 array of two more projectors to increase the brightness two-fold.

The third system is that of a table top vase lit by six projectors (Qumi Q2-B) in a tiled configuration or in superimposed configuration seen by eight cameras Logitech c920 driven by three machines. Fig. 15a shows the system with six projectors in tiled configuration and part b and c shows final result of geometric registration around the vase. Fig. 15d shows the result of superimposed projection on the vase.

The final system is a 90 degrees partial cylinder of 14' radius (22' wide and 6' high) lit by 5×2 array of projectors (EPSON HC1060) seen by four cameras (Logitech c920) and driven by five machines. Fig. 14 shows the result for this system demonstrating the scalability of our method to a large number of projectors and cameras. Fig. 7 shows the projected features during projector movement and the result of the geometric registration after recalibration of moving projector.

Fig. 10 shows the comparison of 3D reconstruction for this setup. The average reconstruction error for a 90 degrees partial cylinder of 14' radius was $0.021'$ which is $\%0.0015$ of the cylinder's radius.

In our experiments we used computers with Intel Core i5 CPU and 8 gigabytes RAM and our unoptimized Matlab implementation takes around 1.5 minutes on the sphere with three projectors and 2 minutes on the sandpit with six projectors. The time breakdown for each step is provided in Table 2. Re-calibration of the projectors takes approximately 10 seconds in our Matlab implementation.

We also evaluated our method in a simulator system that we developed of projectors and cameras. We used OpenGL to render the projected pattern from projectors from view of each individual cameras. Then we used these rendered images to detect the projected binary blobs in image plane of cameras (This causes a trivial amount of error in finding the exact location of the center of each blob). We also used the same technique by rendering a set of images of a checkerboard in order to find an initial value for focal length of cameras as the input of the system instead of using the known value of intrinsic parameters in simulator (We also added radial distortion in

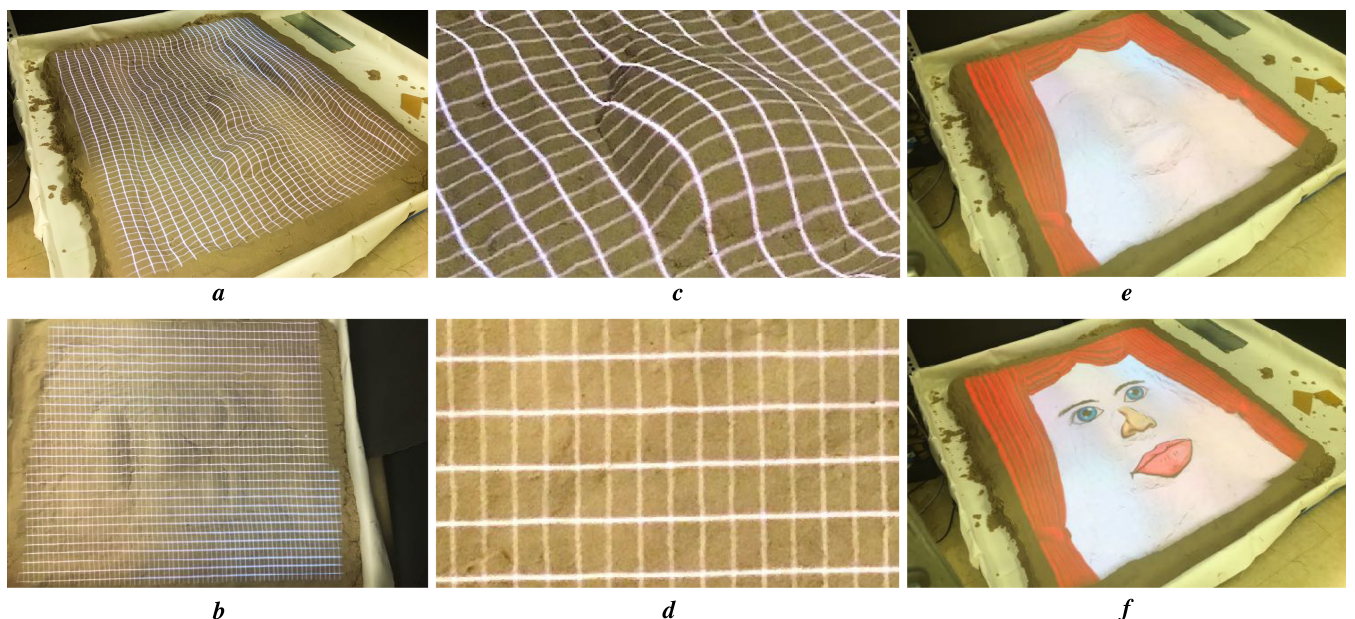


Fig. 13. This figure shows our result projecting on a sand pit using same setup as Fig. 1. (a and b): View-dependent projection from the incorrect view point(a) and correct view position(b). (c and d): Zoomed in image to show the accuracy of geometric registration. (e and f): Shows the result of changing the appearance of display geometry by projecting different contents.



Fig. 14. Top: Showing the overlap of projectors for our setup with 10 projectors and 4 cameras on a cylindrical display surface. Bottom: Final result of projecting a graffiti on the cylindrical wall.



Fig. 15. This figure shows our result on small objects. First row: Our setup with 6 projectors and 8 cameras in tiled configuration around the vase. The projectors illuminate the vase and other objects around it. Second row: Our final result from different view-points. Third row: Showing a checker-board pattern on the vase to demonstrate the accuracy of geometric registration(left) and the result of superimposed projection on the vase (right).

TABLE 2
System Running Time

	Spherical	Sandpit	Vase	Cylindrical
Step 1	30sec	40sec	80sec	100sec
Step 2	35sec	45sec	55sec	70sec
Step 3	15sec	25sec	30sec	45sec
Step 4	15sec	20sec	25sec	35sec
Total Time	$\simeq 1.5\text{min}$	$\simeq 2\text{min}$	$\simeq 3\text{min}$	$\simeq 4\text{min}$

TABLE 3
Comparison of the Estimated Projector Intrinsic (in pixel) Using Checker-Board and our System

		F	Cx	Cy
Projector1	Checkerboard	1941.75	486.93	939.89
	Ours	1924.55	454.9	947.40
Projector2	Checkerboard	2039.72	464.75	648.16
	Ours	1949.43	540.24	703.79
Projector3	Checkerboard	1942.30	544.66	726.43
	Ours	1875.24	537.95	730.91
Projector4	Checkerboard	1803.63	495.32	695.35
	Ours	1747.54	458.81	683.16

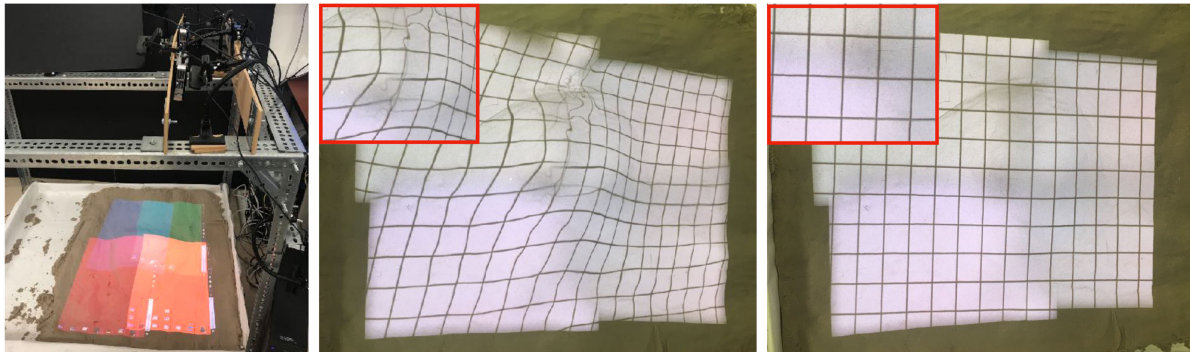


Fig. 16. This figure shows the comparison of our method (right) with result of registration by estimating the device parameters by standard checkerboard calibration method and using this estimation for 3D reconstruction without cross-validation between devices (middle) on a display made of 4 projectors on a sandpit observed by 4 cameras (left).

rendered images). Then we used our method to calibrate all the devices in the simulator and find the 3D coordinates of the display surface. After calibration of the whole system, we projected back the reconstructed 3D coordinates of the points on each projector's image plane. Comparing the calculated coordinates with known coordinates of these points in the projector's image plane, we find that our average reprojection error is 0.44 pixel. Fig. 11 shows the amount of the reprojection error for the 3D points on the image plane of one of the projectors in x and y direction. We also compare the result of our projector calibration with projector calibration method using a checkerboard [54] which is considered as the gold standard reference in the literature [42]. Table 3 show the comparison of estimated results. It is important to note here that there is some deviation of the parameters given by our method from the gold standard. But the deviation is necessary to achieve a consistent parameter reconstruction across multiple devices leading to sub-pixel accuracy in registration. To demonstrate this point we show the registration achieved using the gold standard calibration parameters using the checker-board and our method in Fig. 16. For this purpose we used a checker board to calculate intrinsic parameters of all devices and extrinsic parameters of projectors and cameras with respect to each other. Then we transform all extrinsic parameters to a common global coordinate system and use triangulation method to find the 3D coordinates of pixel correspondences between devices found by binary blob projection. Note that the gold standard parameters lead to tens of pixels registration error while ours yield high accuracy. The pixel misalignment in overlaps and distortion in non-overlapping areas is due to the fact that the reconstructed 3D coordinate of blobs from different projectors will not result in a smooth surface in both overlapping and non-overlapping areas. This shows that our method achieves the optimal balance between consistency of calibration across multiple devices and registration accuracy. Finally, since our method does not need the checker-board, we achieve this calibration completely automatically.

8 CONCLUSION

In conclusion, we present the first work on auto-calibrating projectors on arbitrary 3D shapes using a non-linear projector model common in today's commodity projectors. Our system is accurate, robust and scalable to any number of projectors and cameras. We accurately reconstruct the shape

of the display surface without having at least two observing cameras at each point. Auto-calibration allows for quick recalibration in the face of change in projector position, orientation and zoom factor. However, our method achieves only edge blending which often do not provide complete color seamlessness. We would like to extend more sophisticated centralized color calibration methods such as [3] to a distributed system like ours. Finally, we cannot address colored surface yet which is also one of the future directions of research we would like to pursue. Also our current system can not handle discontinuities in geometry of the display surface such as holes and non-smooth surfaces. We would like to solve this in future as well.

REFERENCES

- [1] R. Raskar et al., "Multi projector displays using camera based registration," in *Proc. IEEE Vis.*, 1999, pp. 161–522.
- [2] A. Majumder and M. Gopi, "Modeling color properties of tiled displays," *Comput. Graphics Forum*, vol. 24, pp. 149–163, Jun. 2005.
- [3] B. Sajadi, M. Lazarov, A. Majumder, and M. Gopi, "Color seamlessness in multi-projector displays using constrained gamut morphing," *IEEE Trans. Vis. Comput. Graphics*, vol. 15, no. 6, pp. 1317–1326, Nov./Dec. 2009.
- [4] R. Raskar, "Immersive planar displays using roughly aligned projectors," in *Proc. IEEE Virtual Reality*, 2000, pp. 109–115.
- [5] A. Raij and M. Polleyfeys, "Auto-calibration of multi-projector display walls," in *Proc. 17th Int. Conf. Pattern Recognit.*, 2004, pp. 14–17.
- [6] A. Raij, G. Gill, A. Majumder, H. Towles, and H. Fuchs, "PixelFlex 2: A comprehensive automatic casually aligned multi-projector display," in *Proc. IEEE Int. Workshop Projector-Camera Syst.*, 2003.
- [7] R. Yang, D. Gotz, J. Hensley, H. Towles, and M. S. Brown, "PixelFlex: A reconfigurable multi-projector display system," in *Proc. IEEE Vis.*, 2001, pp. 167–554.
- [8] E. Bhasker, P. Sinha, and A. Majumder, "Asynchronous distributed calibration for scalable reconfigurable multi-projector displays," *IEEE Trans. Vis. Comput. Graphics*, vol. 12, no. 5, pp. 1101–1108, Sep./Oct. 2006.
- [9] E. Bhasker, R. Juang, and A. Majumder, "Registration techniques for using imperfect and partially calibrated devices in planar multi-projector displays," *IEEE Trans. Vis. Comput. Graphics*, vol. 13, no. 6, pp. 1368–1375, Nov./Dec. 2007.
- [10] H. Chen, R. Sukthankar, G. Wallace, and K. Li, "Scalable alignment of large-format multi-projector displays using camera homography trees," in *Proc. IEEE Vis.*, 2002, pp. 339–346.
- [11] W. B. Seales and M. S. Brown, "A practical and flexible tiled display system," in *Proc. 10th Pacific Conf. Comput. Graphics Appl.*, 2002, pp. 194–203.
- [12] M. Harville, B. Culbertson, I. Sobel, D. Gelb, A. Fitzhugh, and D. Tanguy, "Practical methods for geometric and photometric correction of tiled projector displays on curved surfaces," in *Proc. Conf. Comput. Vis. Pattern Recognit. Workshop*, 2006, p. 5.

- [13] W. Sun, I. Sobel, B. Culbertson, D. Gelb, and I. Robinson, "Calibrating multi-projector cylindrically curved displays for "wallpaper" projection," in *Proc. 5th IEEE/ACM Int. Workshop Projector Camera Syst.*, 2008, Art. no. 1.
- [14] B. Sajadi and A. Majumder, "Markerless view-independent registration of multiple distorted projectors on vertically extruded surface using a single uncalibrated camera," *IEEE Trans. Vis. Comput. Graphics*, vol. 15, no. 6, pp. 1307–1316, Nov. 2009.
- [15] B. Sajadi and A. Majumder, "Scalable multi-view registration for multi-projector displays on vertically extruded surfaces," *Comput. Graphics Forum*, vol. 29, pp. 1063–1072, 2010.
- [16] B. Sajadi and A. Majumder, "Automatic registration of multi-projector domes using a single uncalibrated camera," *Comput. Graphics Forum*, vol. 30, pp. 1161–1170, 2011.
- [17] B. Sajadi and A. Majumder, "Automatic registration of multiple projectors on swept surfaces," in *Proc. 17th ACM Symp. Virtual Reality Softw. Technol.*, 2010, pp. 159–166.
- [18] B. Sajadi and A. Majumder, "Auto-calibrating projectors for tiled displays on piecewise smooth vertically extruded surfaces," *IEEE Trans. Vis. Comput. Graphics*, vol. 17, no. 9, pp. 1209–1222, Sep. 2011.
- [19] R. Raskar, J. V. Baar, T. Willwacher, and S. Rao, "Quadric transfer for immersive curved screen displays," in *Comput. Graphics Forum*, Oxford, UK and Boston, USA: Blackwell Publishing, Inc., vol. 23, no. 3, pp. 451–460, 2004.
- [20] T. Johnson, F. Gyarfas, R. Skarbez, H. Towles, and H. Fuchs, "A personal surround environment: Projective display with correction for display surface geometry and extreme lens distortion," in *Proc. IEEE Virtual Reality Conf.*, 2007, pp. 147–154.
- [21] B. Sajadi, M. A. Tehrani, M. Rehimzadeh, and A. Majumder, "High-resolution lighting of 3D relief maps using a network of projectors and cameras," in *Proc. 3D-TV Conf. Immersive Interactive 3D Media Experience Over Netw.*, 2015, pp. 1–4.
- [22] D. Aliaga and Y. Xu, "Photogeometric structured light: A self-calibrating and multi-viewpoint framework for accurate 3D modeling," in *Proc. IEEE Conf. Comput. Vis. Pattern Recognit.*, 2008, pp. 1–8.
- [23] D. Aliaga, "Digital inspection: An interactive stage for viewing surface details," in *Proc. ACM Symp. Interactive 3D Graphics Games*, 2008, pp. 53–60.
- [24] D. Aliaga, Y. H. Yeung, A. J. Law, B. Sajadi, and A. Majumder, "Fast high-resolution appearance editing using superimposed projections," *ACM Trans. Graphics*, vol. 31, 2012, Art. no. 13.
- [25] A. Law, D. Aliaga, B. Sajadi, A. Majumder, and Z. Pizlo, "Perceptually-based appearance modification for compliant appearance editing," *Comput. Graphics Forum*, vol. 30, pp. 2288–2300, 2011.
- [26] R. Raskar, G. Welch, M. Cutts, A. Lake, L. Stesin, and H. Fuchs, "The office of the future: A unified approach to image based modeling and spatially immersive display," in *Proc. ACM 25th Annu. Conf. Comput. Graphics Interactive Techn.*, 1998, pp. 168–176.
- [27] J. Deglint, F. Li, and H. Sekkati, "Simultaneous projector-camera self-calibration for three-dimensional reconstruction and projection mapping," *IEEE Trans. Comput. Imag.*, vol. 3, no. 1, pp. 74–83, Mar. 2017.
- [28] T. Kanade, S. Yamazaki, and M. Mochimaru, "Simultaneous self-calibration of a projector and a camera using structured light," in *Proc. IEEE Comput. Soc. Conf. Comput. Vis. Pattern Recognit. Workshops*, 2011, pp. 60–67.
- [29] P. S. Huang and S. Zhang, "Novel method for structured light system calibration," *Opt. Eng.*, vol. 45, 2006, Art. no. 083601.
- [30] Z. Li, Y. Shi, C. Wang, and Y. Wangi, "Accurate calibration method for a structured light system," *Opt. Eng.*, vol. 47, 2008, Art. no. 053604.
- [31] S.-Y. Park and G. G. Park, "Active calibration of camera-projector systems based on planar homography," in *Proc. 20th Int. Conf. Pattern Recognit.*, 2010, pp. 320–323.
- [32] J. C. Lee, P. H. Dietz, D. Maynes-Aminzade, R. Raskar, and S. E. Hudson, "Automatic projector calibration with embedded light sensors," in *Proc. 17th Annu. ACM Symp. User Interface Softw. Technol.*, 2004, pp. 123–126.
- [33] J. Liao and L. Cai, "A calibration method for uncoupling projector and camera of a structured light system," in *Proc. IEEE/ASME Int. Conf. Adv. Intell. Mechatronics*, 2008, pp. 770–774.
- [34] J. Geng, T. T. Li, and H. Y. Zhang, "Geometric calibration of a camera-projector 3D imaging system," in *Proc. 25th Int. Conf. Image Vis. Comput. New Zealand*, 2010, pp. 1–8.
- [35] J.-N. Ouellet, F. Rochette, and P. Hebert, "Geometric calibration of a structured light system using circular control points," in *Proc. 3D Data Process. Vis. Transm.*, 2008, pp. 183–190.
- [36] C. Resch, H. Naik, P. Keitler, S. Benkhardt, and G. Klinker, "On-site semi-automatic calibration and registration of a projector-camera system using arbitrary objects with known geometry," *IEEE Trans. Vis. Comput. Graphics*, vol. 21, no. 11, pp. 1211–1220, Nov. 2015.
- [37] G. Moreau, L. Yang, and J.-M. Normand, "Practical and precise projector-camera calibration," in *Proc. IEEE Int. Symp. Mixed Augmented Reality*, 2016, pp. 63–70.
- [38] R. Koch, and O. Fleischmann, "Fast projector-camera calibration for interactive projection mapping," in *Proc. 23rd Int. Conf. Pattern Recognit.*, 2016, pp. 3798–3803.
- [39] B. Sajadi and A. Majumder, "Auto-calibration of cylindrical multi-projector systems," in *Proc. IEEE Virtual Reality Conf.*, 2010, pp. 155–162.
- [40] A. Zakhori, and R. R. Garcia, "Geometric calibration for a multi-camera-projector system," in *Proc. IEEE Workshop Appl. Comput. Vis.*, 2013, pp. 467–474.
- [41] S. Garrido-Jurado, R. Muoz-Salinas, F. Madrid-Cuevas, and M. Marn-Jimnez, "Simultaneous reconstruction and calibration for multi-view structured light scanning," *J. Visual Commun. Image Representation*, vol. 39, pp. 120–131, 2016.
- [42] S. Willi and A. Grundhfer, "Robust geometric self-calibration of generic multi-projector camera systems," in *Proc. IEEE Int. Symp. Mixed Augmented Reality*, 2017, pp. 42–51.
- [43] J. Zhou, L. Wang, A. Akbarzadeh, and R. Yang, "Multi-projector display with continuous self-calibration," in *Proc. IEEE/ACM Workshop Projector-Camera Syst.*, 2008, Art. no. 3.
- [44] R. Yang and G. Welch, "Automatic projector display surface estimation using every-day imagery," in *Proc. 9th Int. Conf. Central Europe Comput. Graphics Vis.*, 2001, pp. 328–335.
- [45] D. Cotting, M. Naes, M. Gross, and H. Fuchs, "Embedding imperceptible patterns into projected images for simultaneous acquisition and display," in *Proc. 3rd IEEE ACM Int. Symp. Mixed Augmented Reality*, 2004, pp. 100–109.
- [46] D. Cotting, R. Ziegler, M. Gross, and H. Fuchs, "Adaptive instant displays: Continuously calibrated projections using per-pixel light control," in *Proc. Eurographics*, 2005, pp. 705–714.
- [47] T. Johnson and H. Fuchs, "Real-time projector tracking on complex geometry using ordinary imagery," in *Proc. IEEE CVPR Workshop Projector Camera Syst.*, 2007, pp. 1–8.
- [48] T. Johnson, G. Welch, H. Fuchs, E. L. Force, and H. Towles, "A distributed cooperative framework for continuous multi-projector pose estimation," in *Proc. IEEE Virtual Reality Conf.*, 2009, pp. 35–42.
- [49] S. Zollmann, T. Langlotz, and O. Bimber, "Passive-active geometric calibration for view-dependent projections onto arbitrary surfaces," in *Proc. Workshop Virtual Augmented Reality GI-Fachgruppe AR/VR*, 2006.
- [50] R. Raskar, J. van Baar, P. Beardsley, T. Willwacher, S. Rao, and C. Forlines, "iLamps: Geometrically aware and self-configuring projectors," *ACM Trans. Graphics*, vol. 22, pp. 809–818, 2003.
- [51] T. Pajdla, M. Bujnak, and Z. Kukelova, "3D reconstruction from image collections with a single known focal length," in *Proc. IEEE 12th Int. Conf. Comput. Vis.*, 2009, pp. 1803–1810.
- [52] S. Cronk, C. Fraser, and H. Hanley, "Automated metric calibration of colour digital cameras," *The Photogrammetric Record*, vol. 21, pp. 355–372, 2006.
- [53] N. Snavely, S. M. Seitz, and R. Szeliski, "Photo tourism: Exploring photo collections in 3D," *ACM Trans. Graphics*, vol. 25, pp. 835–846, 2006.
- [54] D. Moreno and G. Taubin, "Simple, accurate, and robust projector-camera calibration," in *Proc. 3D Data Process. Vis. Transm.*, 2012, pp. 464–471.
- [55] X. Zhang and L. Zhu, "Projector calibration from the camera image point of view," *Opt. Eng.*, vol. 48, 2009, Art. no. 117208.
- [56] P. Roman, M. Lazarov, and A. Majumder, "A scalable distributed paradigm for multi-user interaction with tiled rear projection display walls," *IEEE Trans. Vis. Comput. Graph.*, vol. 16, no. 6, pp. 1623–1632, Nov./Dec. 2010.
- [57] O. Özyesil, V. Voroninski, R. Basri, and A. Singer, "A survey on structure from motion," *Acta Numerica* 26, pp. 305–364, 2017.
- [58] P. Moulon, P. Monasse, and R. Marlet, "Adaptive structure from motion with a contrario model estimation," in *Proc. 11th Asian Conf. Comput. Vis.*, 2013, pp. 257–270.
- [59] J. J. Moré, *The Levenberg–Marquardt Algorithm: Implementation and Theory*. Berlin, Germany: Springer, 1978, pp. 105–116. [Online]. Available: <http://dx.doi.org/10.1007/BFb0067700>

- [60] H. Chen, R. Sukthankar, G. Wallace, and K. Li, "Scalable alignment of large-format multi-projector displays using camera homography trees," in *Proc. Conf. Vis.*, 2002, pp. 339–346.
- [61] H. Chen, R. Sukthankar, G. Wallace, and T. Jen Cham, "Calibrating scalable multi-projector displays using camera homography trees," in *Proc. Conf. Comput. Vis. Pattern Recognit.*, 2001, pp. 9–14.
- [62] O. Bimber, D. Iwai, G. Wetzstein, and A. Grundhöfer, "The visual computing of projector-camera systems," in *Proc. ACM SIGGRAPH Classes*, 2008, Art. no. 84.
- [63] M. Brown, A. Majumder, and R. Yang, "Camera-based calibration techniques for seamless multiprojector displays," *IEEE Trans. Vis. Comput. Graphics*, vol. 11, no. 2, pp. 193–206, Mar./Apr. 2005.
- [64] D. G. Kendall, "A survey of the statistical theory of shape," *Stat. Sci.*, vol. 4, no. 2, pp. 87–99, 1989.
- [65] F. L. Bookstein, "Morphometric tools for landmark data," *Biometrical J.*, vol. 35, no. 4, pp. 512–512, 1993.



Mahdi Abbaspour Tehrani received the BSc degree in computer engineering from the Sharif University of Technology and the PhD degree in computer graphics from the Department of Computer Science, University of California, Irvine, in 2018. His research interests include unified and automatic calibration of spatially augmented reality systems.



M. Gopi received the PhD degree from the University of North Carolina at Chapel Hill. He is currently a professor of computer science with the Department of Computer Science, and associate dean with the Bren School of Information and Computer Sciences, University of California, Irvine. His research interests include geometry and topology in computer graphics, massive geometry data management for interactive rendering, and biomedical sensors, data processing, and visualization.



Aditi Majumder received the PhD degree from the Department of Computer Science, University of North Carolina at Chapel Hill, in 2003. She is currently a professor with the Department of Computer Science, University of California, Irvine. Her research interests include novel displays and cameras exploring new degrees of freedom and quality while keeping them truly commodity, easily accessible to the common man. She is the coauthor of the book *Practical Multi-Projector Display Design*.

▷ For more information on this or any other computing topic, please visit our Digital Library at www.computer.org/csdl.